J Neurophysiol 92: 181–188, 2004.
First published March 3, 2004; 10.1152/jn.00123.2004.

Tissue Resistance Changes and the Profile of Synchronized Neuronal Activity During Ictal Events in the Low-Calcium Model of Epilepsy

John E. Fox, Marom Bikson, and John G. R. Jefferys
Department of Neurophysiology, The Medical School, Division of Neuroscience, University of Birmingham, Birmingham, B15 2TT, United Kingdom

Submitted 5 February 2004; accepted in final form 27 February 2004

Fox, John E., Marom Bikson, and John G. R. Jefferys. Tissue resistance changes and the profile of synchronized neuronal activity during ictal events in the low-calcium model of epilepsy. *J Neurophysiol* 92: 181–188, 2004. First published March 3, 2004; 10.1152/jn.00123.2004. Population spikes vary in size during prolonged epileptic ("ictal") discharges, indicating variations in neuronal synchronization. Here we investigate the role of changes in tissue electrical resistivity in this process. We used the rat hippocampal slice, low-Ca^{2+} model of epilepsy and measured changes in pyramidal layer extracellular resistance during the course of electrographic seizures. During each burst, population spike frequency decreased, whereas amplitude and spatial synchronization increased; after the main discharge, there could be brief secondary discharges that, in contrast with those in the primary discharge, started with high-amplitude population spikes. Mean resistivity increased from 1,231 Ω.cm immediately before the burst to a maximum of 1,507 Ω.cm during the burst. There was no significant increase during the first 0.5–1 s of the field burst, but resistance then increased ($\tau \sim 5$ s), reaching its peak at the end of the burst, and then decayed slowly ($\tau \sim 10$ s). In further experiments, we modulated the efficacy of electrical field effects by changing perfusate osmolarity. Reducing osmolarity by 40–70 mOsm increased preburst resistivity by 19%; it reduced minimum population spike frequency (×0.6–0.7) and increased both maximum population spike amplitude (×1.5–2.3) and spatial synchronization (×1.4–2.5, cross-correlation over 0.5 mm) during bursts. Increasing osmolarity by 20–40 mOsm had the opposite effects. These results suggest that, during each field burst, field effects between neurons gradually become more effective as cells swell, thereby modulating burst dynamics and facilitating the rapid synchronization of secondary discharges.

INTRODUCTION

The pattern of synchronized neuronal activity in an epileptic event changes as the attack progresses. Because synchronization of neuronal discharges can be facilitated by electrical field effects between neurons (Jefferys 1981; Snow and Dudek 1984, 1986; Traub et al. 1985), we have examined the hypothesis that, during the course of the ictal discharge, there may be changes in tissue resistance which modify the efficacy of field effects and hence influence the changing profile of the electrographic seizure.

To eliminate synaptically mediated influences, we used the in vitro low-Ca^{2+} model of epilepsy. In this preparation, the CA1 region of the hippocampal slice, exposed to artificial cerebrospinal fluid (ACSF) containing a low concentration ($\leq$0.2 mM) of Ca^{2+}, generates spontaneous field bursts (Haas and Jefferys 1984; Jefferys and Haas 1982; Konnerth et al. 1984; Taylor and Dudek 1982, 1984a,b), which consist of a slow negative potential lasting several seconds (the "field shift"), superimposed on which there may be population spikes comprising synchronized action potentials (Andersen et al. 1971; Haas and Jefferys 1984; Lopez-Aguado et al. 2002; Varona et al. 2000). The amplitude and frequency of the population spikes change during the course of the discharge (Bikson et al. 2003a,b; Haas and Jefferys 1984; Taylor and Dudek 1984b).

Tissue resistivity increases during epileptic seizures, at least when induced in hippocampal slices in vitro by elevated potassium (Traynelis and Dingledine 1989). Measurements of intrinsic optical signal during epileptic activity in slices suggests a time-dependent shrinkage of the extracellular space fraction (Andrew and MacVicar 1994; Buchheim et al. 2000; Hochman et al. 1995), although the relationship between intrinsic optical signal and extracellular space can be inconsistent and can depend on recording conditions (Buchheim et al. 1999). Any shrinkage of the extracellular space might be expected to modify the strength of field effects between neurons (Ballyk et al. 1991; Dudek et al. 1986). The time course and size of resistivity-changes during epileptic seizures, and their relationship with the profile of neuronal discharges is at present unknown.

Because propagation of epileptic activity across slices can take <1–2 s (Haas and Jefferys 1984; Jefferys and Haas 1982; Konnerth et al. 1984; Yaari et al. 1983), resistance changes due to epileptic activity would be expected to develop at different times in different parts of the slice; moreover, resistivity is known to vary in different layers of the hippocampus, both in vitro and in vivo (Holsheimer 1987; Lopez-Aguado et al. 2001). In the present study, we therefore developed a technique to measure localized resistivity changes in the pyramidal layer while simultaneously recording population spikes from the same electrode to investigate how changes in resistivity, at the level of the cell bodies, correlate with changes in population spikes.

If the profile of neuronal activity is related to localized changes in electrical resistivity, it should be possible to potentiate or oppose the effects by modifying the size of the extracellular space. We induced such changes in slices by modifying the perfusate osmolarity. Changes in osmolarity are known to affect seizure threshold in man and in experimental models of epilepsy (Andrew 1991; Andrew et al. 1989; Roper et al. 1992; Traynelis and Dingledine 1989); in the present study, we

Address reprint requests and other correspondence to: J.G.R. Jefferys (E-mail: j.g.r.jefferys@bham.ac.uk).

The costs of publication of this article were defrayed in part by the payment of page charges. The article must therefore be hereby marked "*advertisement*" in accordance with 18 U.S.C. Section 1734 solely to indicate this fact.

have investigated the effect on the pattern of neuronal activity occurring within ictal events.

METHODS

Transverse hippocampal slices (400 μm) were prepared from male Sprague-Dawley rats (180–225 g; anesthetized with ketamine and medetomidine; killed by cervical dislocation). All experiments were performed under the Animals (Scientific Procedures) Act 1986 of the United Kingdom. The slices were stored, at room temperature, submerged in a holding chamber filled with "normal" ACSF consisting of (in mM) 125 NaCl, 26 $NaHCO_3$, 3 KCl, 2 $CaCl_2$, 1.0 $MgCl_2$, 1.25 NaH_2PO_4, and 10 glucose, aerated with 95% O_2–5% CO_2 mixture. After >60 min, slices were transferred to an interface recording chamber (35°C) containing either normal ACSF or modified ACSF.

Spontaneous activity was induced by perfusion of slices with "low-Ca^{2+}" ACSF consisting of (in mM) 125 NaCl, 26 $NaHCO_3$, 5 KCl, 0.2 $CaCl_2$, 1.0 $MgCl_2$, 1.25 NaH_2PO_4, and 10 glucose, bubbled with 95% O_2–5% CO_2 mixture. Slices generating activity >2 mV in amplitude were accepted in this study (n = 147). Addition of 20–40 mM mannitol to low-Ca^{2+} ACSF produced hyperosmolar perfusates; for hypo-osmolar solutions, NaCl concentration was reduced to 105 and 90 mM (−40 and −70 mOsm). The resistivity of the perfusates was measured using a Conmet 2 Conductivity Meter (Hanna Instruments, Loughborough, UK). The resistivity of (normal osmolar) low-Ca^{2+} and normal ACSF was 63.3 Ω.cm. The resisitivity of −40 mOsm low-Ca^{2+} was 71.4 Ω.cm.

Extracellular field potentials were recorded with glass micropipettes (2–8 MΩ) filled with low-Ca^{2+} ACSF and positioned in the CA1 pyramidal cell layer. Signals were: amplified and low-pass filtered (1–10 kHz) with an Axoclamp-2B or 2A (Axon Instruments) and Neurolog NL-106 and NL-125 amplifiers (Digitimer, Welwyn, UK), digitized using a Power 1401 and Signal and Spike2 software (Cambridge Electronic Design, Cambridge, UK) and analyzed with Signal and Spike2 unless stated otherwise.

A single-micropipette (plus 1 distant return electrode) technique was developed to measure local relative extracellular resistance changes (Fig. 3) using a single standard electrophysiology amplifier (1 channel of an Axoclamp). Fifty-hertz sinusoidal currents (usually ≤5 nA, occasionally ≤10 nA peak-to-peak) were injected into the extracellular micropipette used to record the field potentials (using the amplifier's circuitry); the sensitivity could be adjusted by changing the injected current amplitude. The amplifier's bridge balance was used to adjust the amplitude of the voltage oscillations (during the inter-burst period) to a convenient baseline level. The 50-Hz sinusoidal voltage + the biological signal were then recorded by the *same* field electrode. The 50-Hz component of the trace was then isolated, off-line, using Fourier filter and reconstruction (Autosignal, AISN Software) to identify the changes in extracellular resistance. Similar results were obtained in the time domain by fitting a 50-Hz sinusoid to the combined raw signal to isolate the component due to the applied current, to estimate changes in resistance, and, by subtraction, the biological signal (Spike2 script remsin.exe, Cambridge Electronic Design; scripts are on the web at http://www.ced.co.uk/pru.shtml, under "script library").

To quantify tissue resistance, we used a double-barrelled theta glass micropipette electrode (plus 1 distant return/reference Ag/AgCl electrode) technique modified from Lopez-Aguado et al. (2001); here brief (0.2 s) pulses were injected into one barrel, and the voltage change was measured at the other barrel. The ratio of voltage change measured in the slice to the voltage change measured in the bath perfusate, multiplied by the known resistivity of the bath perfusate, was used to calculate resisitivity. The resistivity of the perfusates was established in separate experiments (see preceding text). The sensitivity of the electrode could change with repeated insertions into the slice (probably due to tissue adhering to the electrode tip), so the 50-Hz voltage amplitude measured in the slice was normalized to the most recent voltage amplitude measured in the bath. With both resistance measurement techniques, the micropipette was inserted >50 μm below the slice surface to increase sensitivity and avoid the high-resistance layer of (damaged) tissue (Lopez-Aguado et al. 2001).

The main advantages of the single electrode technique were: high temporal resolution, up to twice the injected sinusoid frequency; high spatial resolution set by the electrode tip diameter (Lopez-Aguado et al. 2001); the ability to record resistance changes and endogenous electrographic seizures from a single site after appropriate signal filtering; and simplicity of implementation. The single-electrode technique was not used, in the present experiments, to make absolute resistance measurements; these were made using the double-barrelled technique.

Power spectral analysis was used to identify percentage changes in the 50-Hz signal during 0.5-s epochs. "Maximum population spike amplitude" in each burst or period was defined as the mean of the five highest amplitude spikes found; "maximum synchronization" was identified as the strongest cross-correlation of activity at two sites, separated by ~0.5 mm, during any 0.5-s epoch; "minimum population spike frequency" was defined as the lowest average rhythmic frequency recorded in any 0.25-s epoch with spikes >0.7 mV. Amplitude and duration of the slow DC shifts were measured as the mean of >5 bursts. Arrays of three to four electrodes were used to estimate propagation velocities; if the initiation zone was between two electrodes, the velocity was calculated from the delay between electrodes outside this region.

Recordings of extracellular concentration of potassium ions ($[K^+]_o$) were performed using double-barrelled ion-sensitive microelectrodes. One channel was backfilled with low-Ca^{2+} ACSF as the reference channel. The ion-sensing channel was backfilled with 100 mM KCl solution, and its tip was silanized and loaded with a valinomycin ion exchanger (FLUKA 60398). A calibration curve, based on the Nernst equation, was fitted to data for 1, 10, and 100 mM $[K^+]$ (fixed 152.25 mM $[Na^+]$ background) and was used to calculate $[K^+]_o$, which was plotted on a linear scale.

Results are expressed as means ± SE; statistical analyses were made using ANOVA or Student's paired t-test.

RESULTS

Profile of synchronized neuronal discharges

Incubation of slices in low-Ca^{2+} ACSF (>60 min) resulted in the development of spontaneous field bursts in the CA1 region. The average inter-burst interval was 77 ± 11s. Each low-Ca^{2+} burst (Fig. 1) was characterized by a "primary" slow negative field shift; the primary burst duration was 15.9 ± 1.4 s, amplitude was 2.9 ± 0.3 mV, and speed of propagation across the slice was 0.19–2.0 mm/s; the latter was comparable to earlier measurements (Haas and Jefferys 1984). At the end of the field burst, the DC potential returned toward baseline but was frequently interrupted by single or multiple "secondary" slow negative field shifts, which lasted 1–4 s and propagated across the slice at 10–106 mm/s, considerably faster than the primary burst.

The spatiotemporal profile of the first ~1 s of low-Ca^{2+} burst has been described in detail elsewhere (Bikson et al. 2003a). Briefly, population spikes were initially small and relatively irregular with an apparently high frequency; during the first 0.5–1 s, spike size and regularity rapidly increased and frequency decreased. (Fig. 1*B left, bottom trace*).

During the remainder of the primary burst, the DC potential remained stable and had superimposed rhythmic, relatively high-amplitude population spikes (Fig. 1*B*, *middle*) that could

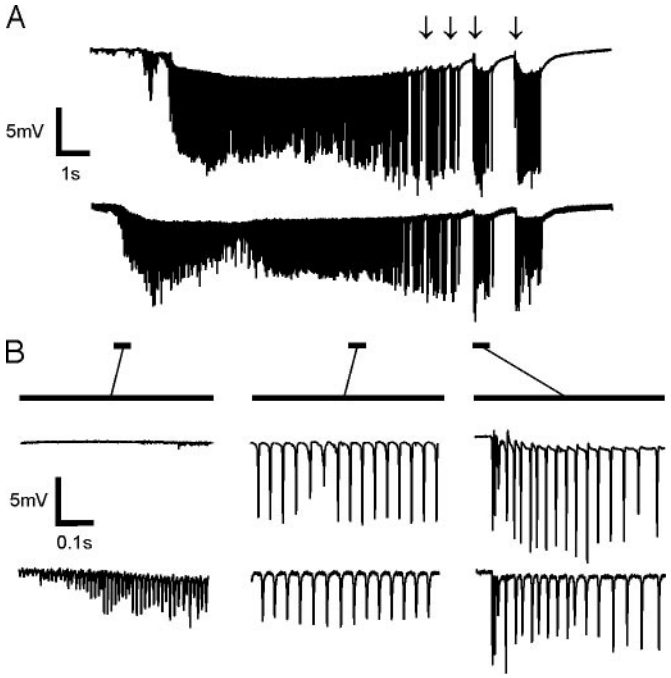

FIG. 1. Low-Ca^{2+} field burst. *A*: low-Ca^{2+} ictal burst, recorded in the CA1 region with 2 field electrodes, separated by ~0.5 mm. Note secondary slow field shifts (↓) in both traces. *B*: expansion of selected regions of burst; *left*: initiation of primary burst; *right*: a secondary burst.

either continue throughout the burst (in 47% of slices) or be interrupted (population spikes <0.7mV) for periods of 2–15 s (in 53% of slices); these are respectively termed "persistent-spiking" and "intermittent bursts" (Bikson et al. 2003b). Even when present continuously, population spike amplitude varied during the burst, tending to decrease toward the middle of the burst and to increase to a maximum at the end of the burst. This terminal increase was evident when rhythmic population spikes were present throughout the final 5 s of the burst (61% of slices): the maximum population spike amplitude (see METHODS) during the first second of this period (5.0 ± 0.42 mV) was less than that during the first 5 s of the whole burst (6.7 ± 0.51 mV) and also less than that during the last 1 s of the primary burst (7.6 ± 0.61 mV; $P < 0.0001$ in both cases; paired *t*-test $n = 46$); maximum population spike amplitude during the last 1 s of the burst exceeded that in the first 5 s in 67% of slices ($P < 0.01$).

At the end of the primary burst, secondary bursts were seen in 33 of 75 slices (Fig. 1*A*, ↓). These contrasted markedly with those in the primary burst in that they started with two or three high-amplitude, high-frequency population spikes, and there was an immediate transition to high-amplitude, low-frequency spiking (Fig. 1*B*, *right*). Population spikes in the secondary bursts had, on average, a higher amplitude than those at the end of the primary burst (maximum spike amplitude during secondary bursts = 9.5 ± 0.81 mV; $P < 0.01$).

Large (>2 mV) population spikes could propagate across the entire CA1 pyramidal cell layer, with propagation velocities of 56–120 mm/s. The average peak correlation coefficient of population spikes in the primary burst, recorded from two sites separated by 0.5 mm, was 0.69 ± 0.05. When a part of CA1 transiently stopped firing, population spike generation on either side of that zone persisted but became desynchronized (Fig. 2).

Tissue resistance changes during the field burst

Absolute resistivity was measured using the two-barrelled micropipette technique (see METHODS). In control ACSF, the average resistance in the pyramidal cell layer was 1,037 ± 250 Ω.cm ($n = 13$) and in the stratum radiatum was 394 ± 121 Ω.cm ($n = 6$); these values are comparable to those obtained by Lopez-Aguado et al. (2001) from slices in an interface chamber. After >60 min exposure to low-Ca^{2+} ACSF, the mean minimum resistivity measured in the pyramidal layer (immediately before the field burst) was 1,231 ± 264 Ω.cm ($n = 15$); during the burst, resistivity increased to a maximum of 1,507 ± 335 Ω.cm ($n = 15$). In low-Ca^{2+} ACSF, measurements were also made in stratum radiatum; at this site, preburst resistivity was 241 ± 99 Ω.cm ($n = 3$), and the maximum resistivity during the burst was 245 ± 106 Ω.cm ($n = 3$). Although there was considerable variability in absolute resistivity measured across slices, at a single location in any given slice, the increase in resistivity during bursts in the pyramidal cell layer was consistent and significant (22 ± 3%, $P < 0.01$).

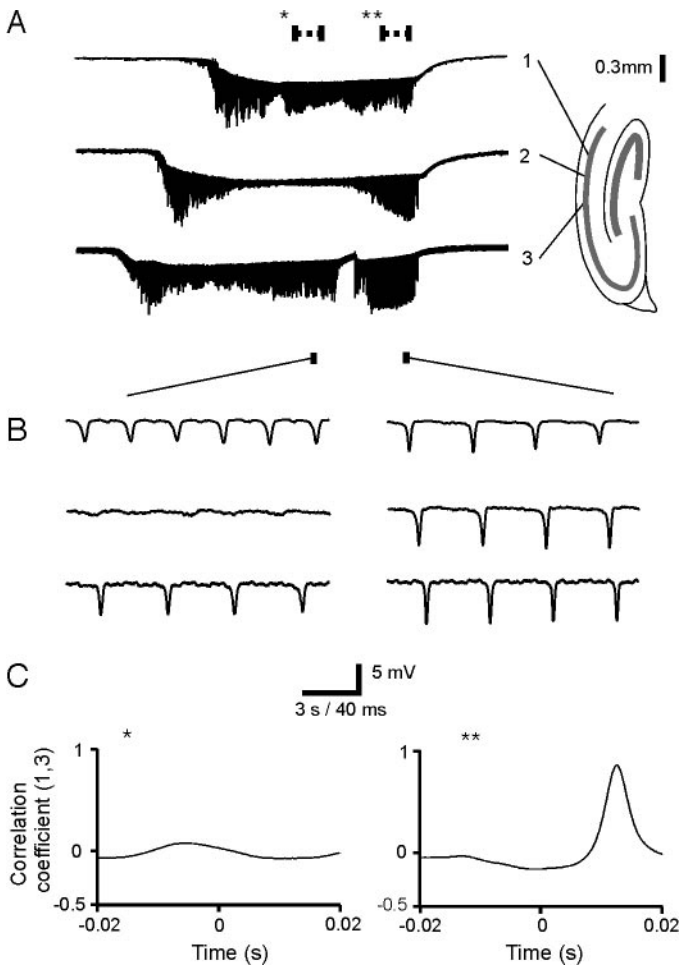

FIG. 2. Effect of local interruption in population spike generation on synchronization across that region. *A*: simultaneous field recording from three sites along the pyramidal cell layer. *B*: expansion of periods where population spikes invade (*right*) and fail to invade (*left*) site 2. *C*: cross-correlation between sites 1 and 3 during periods indicated in *A* by * (*left*) and ** (*right*).

We found no significant difference in resistivity, of either the pyramidal cell layer or stratum radiatum, between slices incubated in normal ACSF and the minimum (preburst) values in slices incubated in low-Ca^{2+} ACSF.

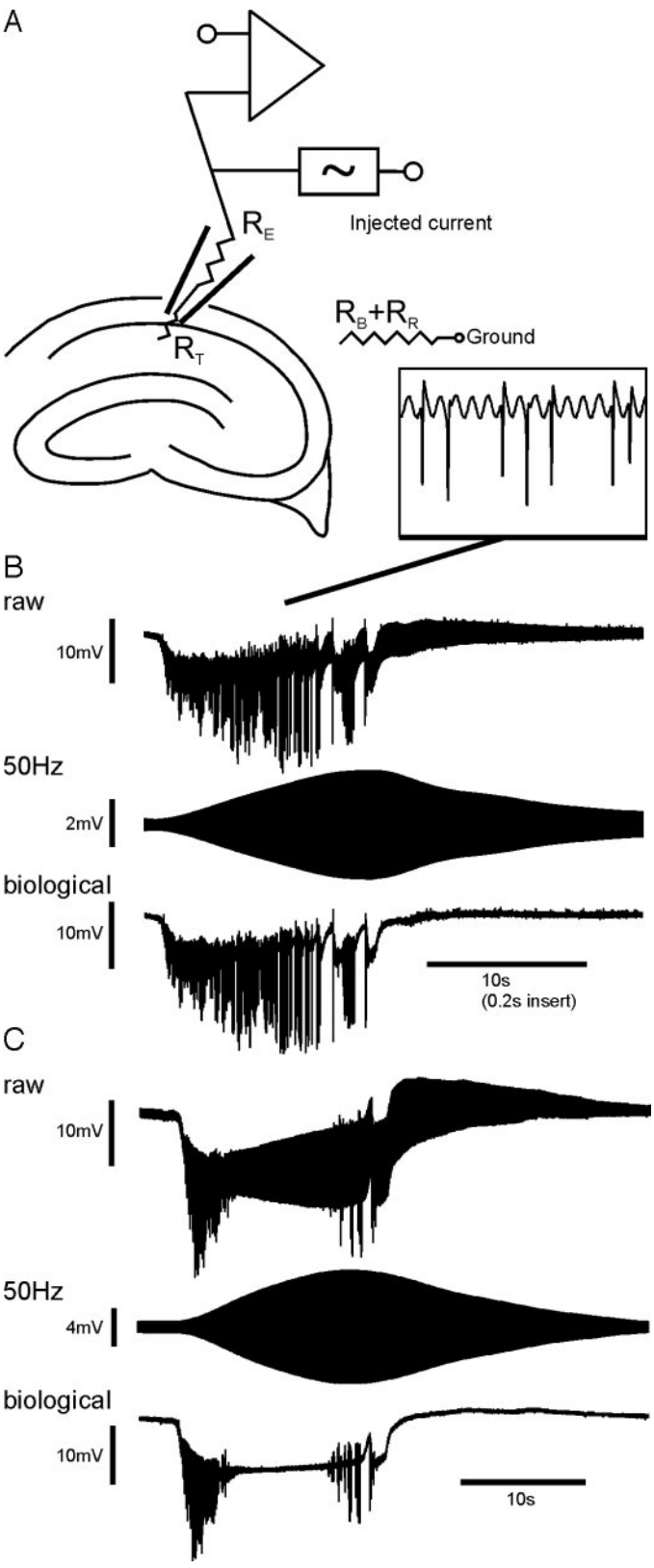

To investigate timing of resistance changes more closely, we assessed changes in extracellular resistance in the pyramidal layer using the experimental set-up shown in Fig. 3 (see METHODS). Sinusoidal currents were injected into a single field micropipette electrode, which was simultaneously used to detect both endogenous voltage changes (i.e., electrographic seizures) and the sinusoidal voltage changes, produced by the applied current, due to any alteration in extracellular resistance; the latter depends linearly on the injected current and on the resistance of the electrode, the slice tissue, bath ACSF, and return electrode (Fig. 3*A*). During recording of low-Ca^{2+} bursts, the only resistance that changes is that of the tissue.

No detectable increase in tissue resistance was observed before burst initiation or during the first 0.5–1 s of the burst (this was confirmed by measuring power at 50 Hz in spectral analysis of the raw trace). During the main part of the burst, however, there was a gradual ($\tau \sim 5$ s) increase in tissue resistance (Fig. 3*B*, *middle*); power spectral analysis showed that the maximum value was reached within 0.5 s of the end of the primary burst (when no secondary bursts followed) or within 0.5 s of the onset of the final secondary burst. The same pattern of increasing resistance was seen during both persistent spiking and intermittent spiking bursts (Fig. 3, *B* and *C*) and so did not depend on continued population spike firing. Tissue resistance decayed slowly ($\tau \sim 10$ s) back to baseline after the termination of the burst.

Changing perfusate osmolarity, effect on population spike characteristics

Osmolarity was increased by addition of mannitol, a membrane-impermeant solute and decreased by removal of NaCl, to produce osmotic challenges ranging from +40 to −70 mOsm (see METHODS). In 6 of 31 slices tested, increasing osmolarity by 30−40 mOsm abolished spontaneous bursting, similar to the results of Dudek et al. (1990). In the remaining slices, however, bursts were still present, albeit with an increase in inter-burst interval and decrease in amplitude of the negative field shift (200 ± 37 and 94 ± 2% control, respectively, during exposure to +40 mOsm). Conversely, decreasing osmolarity decreased interburst interval and increased the amplitude of the negative field shift (69 ± 10 and 140 ± 15% control, respectively, during exposure to −40 mOsm).

The main purpose of these experiments was to determine the effects of exogenous changes in osmolarity on the profile of synchronized neuronal activity within the burst; detailed results are given in Fig. 4. Reducing osmolarity increased the maximum population spike amplitude and lowered the minimum discharge frequency observed during each burst; these effects could be reversed by restoring osmolarity to normal levels

FIG. 3. Tissue resistance changes. *A*: schematic of experimental set-up; circuitry was contained within an Axoclamp working in bridge mode. Current was injected into the field electrode, which was used to monitor field and extracellular resistance changes. R_E, R_T, R_B, R_R are electrode, tissue, bath, and return electrode resistance, respectively. *B* and *C*: ("raw") recording of a field burst during the application of a 50-Hz current through the field electrode (expanded *inset* shows combined applied sinusoidal and biological components in more detail); ("50 Hz") isolation of the 50-Hz component (activity <49 and >51 Hz removed using Fourier filter and reconstruction); ("biological") reconstruction of the physiological signal (49- to 51-Hz activity removed from the raw trace). *B*: a field burst in which spike generation was continuous; *C*: an example of a burst in which spike generation was interrupted.

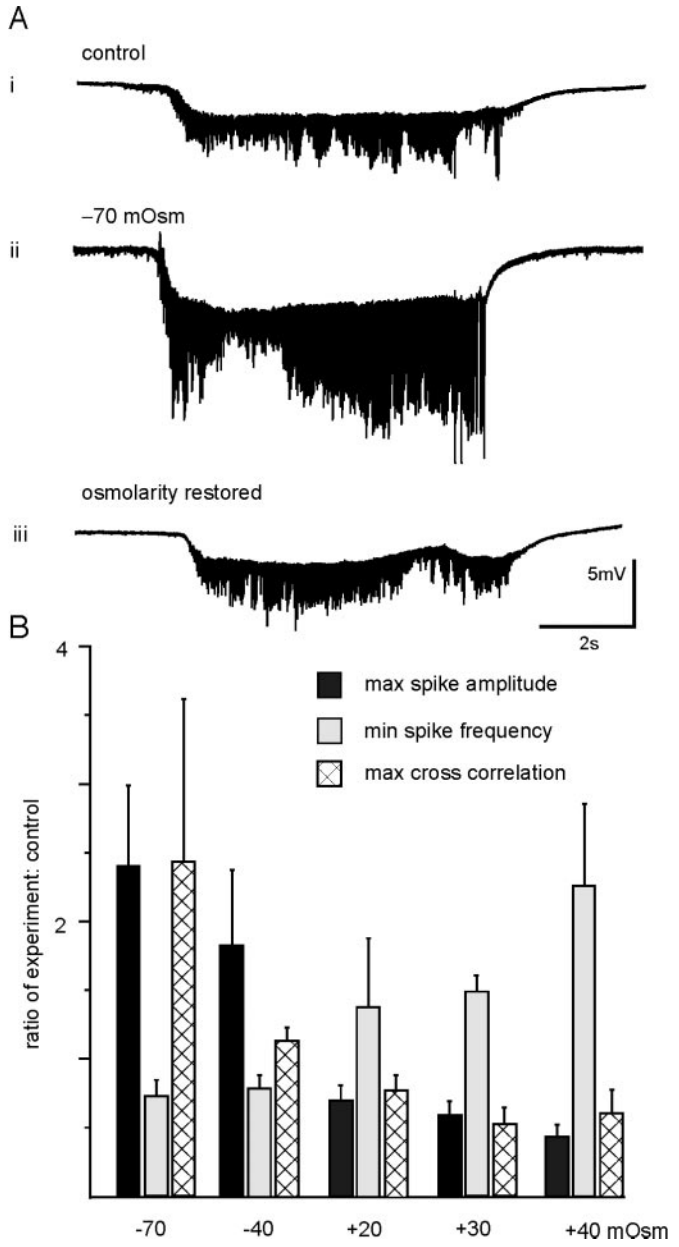

FIG. 4. Effect of changes in osmolarity on low-Ca^{2+} field bursts. *A*: field bursts recorded during perfusion with standard artificial cerebrospinal fluid (ACSF; *i*) and perfusion with reduced [NaCl] (−70 mOsm) (*ii*) and after restoration of osmolarity with mannitol (*iii*). *B*: pooled results summarizing the effects of osmotic challenge on: maximum population spike amplitude (mean control = 5.9 mV); minimum population spike frequency (mean control = 26 Hz) and maximum cross-correlation of activity at 2 sites separated by 0.5 mm (mean control = 0.7). Slices in which activity was completely suppressed by increasing osmolarity are not included. (30 slices; bars show SE; ANOVA shows that osmolarity significantly affects each of these measures, $P < 0.01$.)

either by replacing NaCl or by adding 40 or 70 mM mannitol. Conversely, increasing osmolarity resulted in a reduction in maximum population spike amplitude and a higher final discharge frequency.

The effect of changing osmolarity on synchronization of neuronal activity across the slice was determined by identifying the maximum cross-correlation of activity at two sites, separated by ~0.5 mm (see METHODS). Decreasing osmolarity increased the maximum synchronization of population spike discharges at the two sites, while increasing osmolarity decreased the degree of synchronization (Fig. 4).

Changing perfusate osmolarity; effect on tissue resistance

Decreasing osmolarity by 40 mOsm ($n = 4$) increased the resistivity of the ACSF in the bath by 13% (see METHODS). Decreasing osmolarity by 40 mOsm increased pyramidal layer resistivity during the preburst and end-of-burst periods by 28 and 32%, respectively [compared with measurements made during perfusion with normal osmolar low-calcium ACSF; $P < 0.05$, $n = 7$; comparable changes have previously been described for submerged slices (Andrew et al. 1997)].

Timing of resistance changes during the burst were again monitored with sinusoidal current injection into the recording channel. During perfusion with hypo-osmolar ACSF, the transition to high-amplitude spike generation was faster (Bikson et al. 2003a), but, as in the experiments with normal osmolar ACSF, tissue resistance did not increase during the period leading up to field bursts nor during the first 500 ms of the burst.

Changing perfusate osmolarity; effect on extracellular potassium transients

It has been suggested that osmotic changes would modulate extracellular ionic transients (Andrew et al. 1989; Jefferys 1995); however, this proposition has not been previously tested directly. We measured the changes in extracellular potassium concentration associated with low-Ca^{2+} ictal bursts before and during reductions in extracellular osmolarity. We found that decreasing osmolarity (−70 mOsm) increased peak potassium transient amplitude by 13 ± 4% ($P < 0.05$); its duration increased by 45 ± 18% ($P = 0.057$; Fig. 5; $n = 4$). Reducing osmolarity by 70 and 40 mOsm (by removing NaCl) also led to the development of spreading depression in 16 of 18 and 5 of 6 slices tested, respectively, consistent with enhanced extracellular potassium accumulation (Kager et al. 2000).

DISCUSSION

During each low-Ca^{2+} field burst, extracellular K^+ concentration increased, contributing to the slow negative potential recorded by field electrodes (Haas and Jefferys 1984; Yaari et al. 1983). The decreased transmembrane K^+ gradient causes an increase in neuronal excitability. This is not manifest, however, as random firing of individual neurons; rather, neuronal discharges become synchronized, giving rise to population spikes (Haas and Jefferys 1984; Jefferys 1995; Jefferys and Haas 1982; Patrylo et al. 1996; Taylor and Dudek 1984a,b). Because the Ca^{2+} concentration in the ACSF is below that needed for chemical synaptic transmission (Jones and Heinemann 1987), synchronization must be mediated by nonsynaptic mechanisms.

We have previously shown that during the early part of the field burst, population spikes develop as a result of synchronized discharges in progressively enlarging neuronal aggregates; as the number of neurons recruited into an aggregate increases, the field potential produced by that aggregate increases, resulting in still further recruitment of neurons into the discharging populations (Bikson et al. 2003a). In the present experiments, we show that, at this stage (i.e., during the 1st

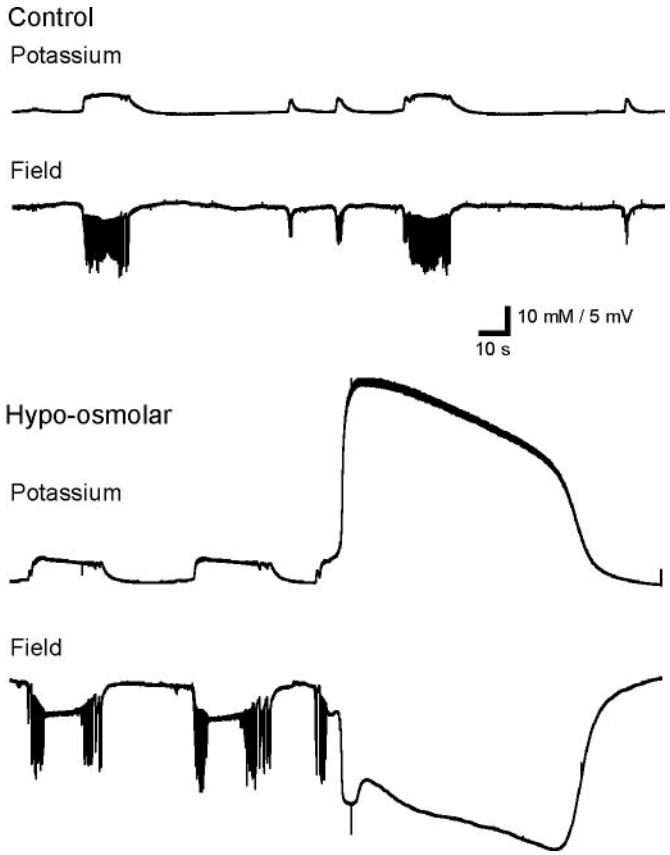

FIG. 5. Effect of osmotic challenge on potassium transients. Field (*bottom*) and potassium-selective (*top*) recordings from the CA1 pyramidal cell layer, during perfusion with low-Ca^{2+} ACSF (baseline value of K^+ was 5 mM in both cases; K^+ has been calculated from the ion-selective recordings and is plotted on a linear scale). Effect of reducing osmolarity by removal of 20 mM NaCl from the perfusate. In this example, reduction of perfusate osmolarity led to spreading depression (end of trace).

0.5–1 s), there is no detectable increase in tissue resistance, and hence the initial recruitment into neuronal aggregates depends on the electrical potential generated by increasing numbers of synchronously activated neurons, not on a change in the efficacy of field effect interactions.

We present evidence that tissue resistance, and therefore by implication the efficacy of field effects, increases gradually during the remainder of the primary burst; the effect of this change would be to increase population spike size as the burst progresses. Intense neuronal activity, as occurs during epileptic events, is associated with swelling (Andrew and MacVicar 1994; Andrew et al. 1997; Buchheim et al. 1999), which brings cell bodies closer together, resulting in a reduction in the extracellular space fraction (Andrew et al. 1996; Holthoff and Witte 1996; Weissinger et al. 2000) and the increase in resistance measured in the present experiments (the applied current flow being predominantly extracellular). Although the changes in the extracellular compartment during neuronal activity are complex (Kume-Kick et al. 2002), the increased proximity of neurons and the increased extracellular resistance within the pyramidal layer will increase the efficacy of field effects between adjacent somata (Lopez-Aguado et al. 2002; Richardson et al. 1984; Taylor and Dudek 1984a; Traub et al. 1985; Varona et al. 2000).

The steady increase in resistance during each field burst tends to increase population spike amplitude, but it is not the only factor determining spike amplitude. We have shown elsewhere that spike generation during low-Ca^{2+} field bursts can be interrupted for prolonged periods as a result of depolarization block (Bikson et al. 2003b). We suggest that the final profile of synchronized neuronal activity during the main phase of the field burst is determined by the interaction of these two opposing influences, enhanced field potentials tending to increase the number of neurons participating in each synchronized discharge, whereas depolarization block tends to reduce the number of neurons able to generate action potentials.

We found that resistance in the pyramidal layer continued to increase even during periods when neuronal firing was completely blocked. This implies that continued ion fluxes, even in the absence of action potential generation (Bikson et al. 2003b), suffice to maintain neuronal swelling with the result that enhanced field effects are still observed when and if neuronal firing returns at the end of the burst.

After the primary burst (i.e., after the DC shift starts to return toward baseline), secondary bursts were frequently seen. In marked contrast to the primary discharge, population potentials characteristically had high amplitudes from the onset (maximum population spike amplitude was 25% greater than that at the end of the primary burst) and propagated rapidly through the slice. The present experiments suggest that this results from the enhanced field effects which develop through the course of the field burst as a result of neuron swelling.

Neuron swelling and shrinkage of the extracellular space can also be induced by experimentally applied changes in osmolarity (Dudek et al. 1990; Kume-Kick et al. 2002; Roper et al. 1992); if direct electrical interactions have an important role in shaping the neuronal discharge during a field burst, changes in osmolarity, by modifying the efficacy of these interactions, would be expected to affect the amplitude of population spikes and the correlation of spike discharges recorded across the slice. These predictions were confirmed in the present experiments (Fig. 4). In addition, we have shown (Fig. 2) that, if part of a slice transiently failed to generate population spikes, regions on either side of that area continued to generate rhythmic population potentials, but they were no longer correlated; this observation is consistent with the hypothesis that synchronization across the slice depends on the continuous conduction of field potentials through adjacent regions of CA1.

Although it is likely that the effects of osmotic change reported here are largely mediated by changes in the extracellular space (Andrew and MacVicar 1994; Andrew et al. 1997; Dudek et al. 1990), modifying osmolarity can have other effects on neuronal excitability (Azouz et al. 1997; Huang and Somjen 1997; Wan et al. 1999). Higher modifications of osmolar concentration can affect membrane properties, but changes of $<$40 mOsm (which had a marked effect in our experiments) are reported not to affect membrane properties (Azouz et al. 1997; Ballyk et al. 1991). Neuronal gap junctions may contribute to synchrony (Traub et al. 1985; Valiante et al. 1995; Vigmond et al. 1997), but it is not established that gap junctions between neurons [as opposed to those between glia (Scemes and Spray 1998)] are affected by cell swelling or changes in osmolarity. Decreasing the extracellular space fraction does, however, cause an increase in extracellular potas-

sium transients that will increase excitability; in the present experiments, this mechanism would contribute to the observed changes in the amplitude of the slow field shift (Dietzel et al. 1989). The increased size of population spikes, however, requires not only that excitability of individual neurons increases but that the action potentials are synchronized. Shrinking the extracellular space enhances field effects between neurons and could account for the increase in synchronization and growth in the amplitude of population spikes that occurs, despite the opposing influence of depolarization block, during the course of ictal discharges.

ACKNOWLEDGMENTS

Spike2 script was courtesy of G. Smith, Cambridge Electronic Design.

Present address: M. Bikson, Dept. of Biomedical Engineering, City College of New York, Convent Ave. and 140th St., New York, New York 10031.

GRANTS

This work was supported in part by the Medical Research Council of the United Kingdom.

REFERENCES

Andersen P, Bliss TVP, and Skrede KK. Unit analysis of hippocampal polulation spikes. *Exp Brain Res* 13: 208–221, 1971.

Andrew RD. Seizure and acute osmotic change: clinical and neurophysiological aspects. *J Neurol Sci* 101: 7–18, 1991.

Andrew RD, Adams JR, and Polischuk TM. Imaging NMDA- and kainate-induced intrinsic optical signals from the hippocampal slice. *J Neurophysiol* 76: 2707–2717, 1996.

Andrew RD, Fagan M, Ballyk BA, and Rosen AS. Seizure susceptibility and the osmotic state. *Brain Res* 498: 175–180, 1989.

Andrew RD, Lobinowich ME, and Osehobo EP. Evidence against volume regulation by cortical brain cells during acute osmotic stress. *Exp Neurol* 143: 300–312, 1997.

Andrew RD and MacVicar BA. Imaging cell volume changes and neuronal excitation in the hippocampal slice. *Neuroscience* 62: 371–383, 1994.

Azouz R, Alroy G, and Yaari Y. Modulation of endogenous firing patterns by osmolarity in rat hippocampal neurons. *J Physiol* 502: 175–187, 1997.

Ballyk BA, Quackenbush SJ, and Andrew RD. Osmotic effects on the CA1 neuronal population in hippocampal slices with special reference to glucose. *J Neurophysiol* 65: 1055–1066, 1991.

Bikson M, Fox JE, and Jefferys JGR. Neuronal aggregate formation underlies spatiotemporal dynamics of nonsynaptic seizure initiation. *J Neurophysiol* 89: 2330–2333, 2003a.

Bikson M, Hahn PJ, Fox JE, and Jefferys JGR. Depolarization block of neurons during maintenance of electrographic seizures. *J Neurophysiol* 90: 2402–2408, 2003b.

Buchheim K, Schuchmann S, Siegmund H, Gabriel HJ, Heinemann U, and Meierkord H. Intrinsic optical signal measurements reveal characteristic features during different forms of spontaneous neuronal hyperactivity associated with ECS shrinkage in vitro. *Eur J Neurosci* 11: 1877–1882, 1999.

Buchheim K, Schuchmann S, Siegmund H, Weissinger F, Heinemann U, and Meierkord H. Comparison of intrinsic optical signals associated with low Mg^{2+}-and 4-aminopyridine-induced seizure-like events reveals characteristic features in adult rat limbic system. *Epilepsia* 41: 635–641, 2000.

Dietzel I, Heinemann U, and Lux HD. Relations between slow extracellular potential changes, glial potassium buffering, and electrolyte and cellular volume changes during neuronal hyperactivity in cat brain. *Glia* 2: 25–44, 1989.

Dudek FE, Obenaus A, and Tasker JG. Osmolality-induced changes in extracellular volume alter epileptiform bursts independent of chemical synapses in the rat: importance of non-synaptic mechanisms in hippocampal epileptogenesis. *Neurosci Lett* 120: 267–270, 1990.

Dudek FE, Snow RW, and Taylor CP. Role of electrical interactions in synchronization of epileptiform bursts. *Adv Neurol* 44: 593–617, 1986.

Haas HL and Jefferys JGR. Low-calcium field burst discharges of CA1 pyramidal neurones in rat hippocampal slices. *J Physiol* 354: 185–201, 1984.

Hochman DW, Baraban SC, Owens JW, and Schwartzkroin PA. Dissociation of synchronization and excitability in furosemide blockade of epileptiform activity. *Science* 270: 99–102, 1995.

Holsheimer J. Electrical conductivity of the hippocampal CA1 layers and application to current-source-density analysis. *Exp Brain Res* 67: 402–410, 1987.

Holthoff K and Witte OW. Intrinsic optical signals in rat neocortical slices measured with near-infrared dark-field microscopy reveal changes in extracellular space. *J Neurosci* 16: 2740–2749, 1996.

Huang R and Somjen GG. Effects of hypertonia on voltage-gated ion currents in freshly isolated hippocampal neurons, and on synaptic currents in neurons in hippocampal slices. *Brain Res* 748: 157–167, 1997.

Jefferys JGR. Influence of electric fields on the excitability of granule cells in guinea pig hippocampal slices. *J Physiol* 319: 143–152, 1981.

Jefferys JGR. Non-synaptic modulation of neuronal activity in the brain: electric currents and extracellular ions. *Physiol Rev* 75: 689–723, 1995.

Jefferys JGR and Haas HL. Synchronized bursting of CA1 pyramidal cells in the absence of synaptic transmission. *Nature* 300: 448–450, 1982.

Jones RSG and Heinemann U. Abolition of the orthodromically evoked IPSP of CA1 pyramidal cells before the EPSP during washout of calcium from hippocampal slices. *Exp Brain Res* 65: 676–680, 1987.

Kager H, Wadman WJ, and Somjen GG. Simulated seizures and spreading depression in a neuron model incorporating interstitial space and ion concentrations. *J Neurophysiol* 84: 495–512, 2000.

Konnerth A, Heinemann U, and Yaari Y. Slow transmission of neural activity in hippocampal area CA1 in absence of active chemical synapses. *Nature* 307: 69–71, 1984.

Kume-Kick J, Mazel T, Vorisek I, Hrabetova S, Tao L, and Nicholson C. Independence of extracellular tortuosity and volume fraction during osmotic challenge in rat neocortex. *J Physiol* 542: 515–527, 2002.

Lopez-Aguado L, Ibarz JM, and Herreras O. Activity-dependent changes of tissue resistivity in the CA1 region in vivo are layer-specific: modulation of evoked potentials. *Neuroscience* 108: 249–262, 2001.

Lopez-Aguado L, Ibarz JM, Varona P, and Herreras O. Structural inhomogeneities differentially modulate action currents and population spikes initiated in the axon or dendrites. *J Neurophysiol* 88: 2809–2820, 2002.

Patrylo PR, Kuhn AJ, Schweitzer JS, and Dudek FE. Multiple-unit recordings during slow field-potential shifts in low-$[Ca^{2+}]_o$ solutions in rat hippocampal and cortical slices. *Neuroscience* 74: 107–118, 1996.

Richardson TL, Turner RW, and Miller JJ. Extracellular fields influence transmembrane potentials and synchronization of hippocampal neuronal activity. *Brain Res* 294: 255–262, 1984.

Roper SN, Obenaus A, and Dudek FE. Osmolality and nonsynaptic epileptiform bursts in rat CA1 and dentate gyrus. *Ann Neurol* 31: 81–85, 1992.

Scemes E and Spray DC. Increased intercellular communication in mouse astrocytes exposed to hyposmotic shocks. *Glia* 24: 74–84, 1998.

Snow RW and Dudek FE. Electrical fields directly contribute to action potential synchronization during convulsant-induced epileptiform bursts. *Brain Res* 323: 114–118, 1984.

Snow RW and Dudek FE. Evidence for neuronal interactions by electrical field effects in the CA3 and dentate regions of rat hippocampal slices. *Brain Res* 367: 292–295, 1986.

Taylor CP and Dudek FE. Synchronous neural afterdischarges in rat hippocampal slices without active chemical synapses. *Science* 218: 810–812, 1982.

Taylor CP and Dudek FE. Excitation of hippocampal pyramidal cells by an electrical field effect. *J Neurophysiol* 52: 126–142, 1984a.

Taylor CP and Dudek FE. Synchronization without active chemical synapses during hippocampal afterdischarges. *J Neurophysiol* 52: 143–155, 1984b.

Traub RD, Dudek FE, Snow RW, and Knowles WD. Computer simulations indicate that electrical field effects contribute to the shape of the epileptiform field potential. *Neuroscience* 15: 947–958, 1985.

Traynelis SF and Dingledine R. Role of extracellular space in hyperosmotic suppression of potassium-induced electrographic seizures. *J Neurophysiol* 61: 927–938, 1989.

Valiante TA, Perez-Velazquez JL, Jahromi SS, and Carlen PL. Coupling potentials in CA1 neurons during calcium-free-induced field burst activity. *J Neurosci* 15: 6946–6956, 1995.

Varona P, Ibarz JM, Lopez-Aguado L, and Herreras O. Macroscopic and subcellular factors shaping population spikes. *J Neurophysiol* 83: 2192–2208, 2000.

Vigmond EJ, Perez VJ, Valiante TA, Bardakjian BL, and Carlen PL. Mechanisms of electrical coupling between pyramidal cells. *J Neurophysiol* 78: 3107–3116, 1997.

Wan X, Juranka P, and Morris CE. Activation of mechanosensitive currents in traumatized membrane. *Am J Physiol Cell Physiol* 276: C318–C327, 1999.

Weissinger F, Buchheim K, Siegmund H, Heinemann U, and Meierkord H. Optical imaging reveals characteristic seizure onsets, spread patterns, and propagation velocities in hippocampal-entorhinal cortex slices of juvenile rats. *Neurobiol Dis* 7: 286–298, 2000.

Yaari Y, Konnerth A, and Heinemann U. Spontaneous epileptiform activity of CA1 hippocampal neurons in low extracellular calcium solutions. *Exp Brain Res* 51: 153–156, 1983.